Intercomparison of O_2/N_2 Ratio Scales Among AIST, NIES, TU, and SIO Based on Round-robin Exercise Using Gravimetric Standard Mixtures

Nobuyuki Aoki[1], Shigeyuki Ishidoya[2], Yasunori Tohjima[3], Shinji Morimoto[4], Ralph F. Keeling[5], Adam Cox[5], Shuichiro Takebayashi[4] and Shohei Murayama[2]

[1]National Metrology Institute of Japan (NMIJ), National Institute of Advanced Industrial Science and Technology (AIST), 1-1-1 Umezono, Tsukuba 305-8563, Japan
[2]Research Institute for Environmental Management Technology (EMRI), National Institute of Advanced Industrial Science and Technology (AIST), Tsukuba 305-8569, Japan
[3]Center for Environmental Measurement and Analysis, National Institute for Environmental Studies, Tsukuba 305-8506, Japan
[4]Center for Atmospheric and Oceanic Studies, Graduate School of Science, Tohoku University, Sendai 980-8578, Japan
[5]Scripps Institution of Oceanography, La Jolla, CA 92093-0244, USA

Correspondence to: Nobuyuki Aoki (aoki-nobu@aist.go.jp)

Abstract. A study was conducted to compare the $\delta(O_2/N_2)$ scales used by four laboratories engaged in atmospheric $\delta(O_2/N_2)$ measurements. These laboratories are the Research Institute for Environmental Management Technology, Advanced Industrial Science and Technology (EMRI/AIST), the National Institute for Environmental Studies (NIES), Tohoku University (TU), and Scripps Institution of Oceanography (SIO). Therefore, five high-precision standard mixtures for O_2 molar fraction gravimetrically prepared by the National Metrology Institute of Japan (NMIJ), AIST (NMIJ/AIST) with a standard uncertainty of less than 5 per meg were used as round-robin standard mixtures. EMRI/AIST, NIES, TU, and SIO reported the analysed values of the standard mixtures on their own $\delta(O_2/N_2)$ scales, and the values were compared with the $\delta(O_2/N_2)$ values gravimetrically determined by NMIJ/AIST (the NMIJ/AIST scale). The $\delta(O_2/N_2)$ temporal drift in the five standard mixtures during the intercomparison experiment from May 2017 to March 2020 was corrected based on the $\delta(O_2/N_2)$ values analysed before and after the laboratory measurements by EMRI/AIST. The scales are compared based on offsets in zero and span. The relative span offsets of EMRI/AIST, TU, NIES, and SIO scales against the NMIJ/AIST scale were −0.11 ± 0.10, −0.10 ± 0.13, 3.39 ± 0.13, and 0.93 ± 0.10 %, respectively. The largest offset corresponded with a 0.30 Pg yr^{-1} decrease and increase in global estimates for land biospheric and oceanic CO_2 uptakes based on trends in atmospheric CO_2 and $\delta(O_2/N_2)$. The deviations in the measured $\delta(O_2/N_2)$ values on the laboratory scales from the NMIJ/AIST scale are 65.8 ± 2.2, 425.7 ± 3.1, 404.5 ± 3.0, and 596.4 ± 2.4 per meg for EMRI/AIST, TU, NIES, and SIO, respectively. The difference between atmospheric $\delta(O_2/N_2)$ values observed at Hateruma Island (HAT; 24.05°N, 123.81°E), Japan, by EMRI/AIST and NIES reduced from −329.3 ± 6.9 per meg to −6.6 ± 6.8 per meg by converting their scales to the NMIJ/AIST scale.

1. Introduction

Observing the long-term change in atmospheric O_2 molar fraction, combined with CO_2 observation, enables us to estimate terrestrial biospheric and oceanic CO_2 uptakes separately (Manning and Keeling, 2006; Tohjima et al., 2008; Ishidoya et al., 2012a, 2012b). O_2 is exchanged with CO_2 with distinct stoichiometric ratios for terrestrial biospheric activities and fossil fuel combustion (Keeling, 1988a; Severinghaus. 1995). Meanwhile, the ocean CO_2 uptake and O_2 emissions are decoupled since the ocean acts as a carbon sink by physiochemically dissolving the CO_2 (e.g., Keeling et al., 1993). Various laboratories have performed measurements of atmospheric O_2 since the early 1990s (e.g., Keeling et al., 1996; Bender et al., 2005; Manning and Keeling, 2006; Tohjima et al., 2008, 2019; Ishidoya et al., 2012a, b; Goto et al., 2017). Recently, Resplandy et al. (2019) introduced a method to estimate the global ocean heat content (OHC) increase based on atmospheric O_2 and CO_2 measurements. They extracted solubility-driven components of the atmospheric potential oxygen (APO = O_2 + 1.1 × CO_2) (Stephens et al., 1998) by combining their observational results with climate and ocean models. The global OHC change is a fundamental measure of global warming. Indeed, the ocean takes in more than 90% of the Earth's excess energy as evaluated based on ocean temperature measurements using Argo floats (e.g., Levitus et al., 2012). Thus, the atmospheric O_2 measurements are linked to the global CO_2 budget and OHC.

The approaches described above rely on precise measurements that can detect micro-mole-per-mole-level changes in atmospheric O_2 molar fraction (~21%). After Keeling and Shertz (1992) succeeded in developing the measurement technique based on the interferometer, various measurement techniques have been developed to quantify atmospheric O_2 molar fraction, including using mass spectrometry (Bender et al., 1994; Ishidoya et al., 2003; Ishidoya and Murayama, 2014), a paramagnetic technique (Manning et al., 1999; Ishidoya et al., 2017; Aoki and Shimosaka, 2018), a vacuum-ultraviolet absorption technique (Stephens et al., 2003), gas chromatography (Tohjima, 2000), a method using fuel cells (Stephens et al., 2007; Goto et al., 2013), and a cavity ring-down spectroscopy analyser (Berhanu et al., 2019). All programs have reported changes in O_2 regarding the equivalent changes in the O_2/N_2 ratio by convention. This is expressed as the relative change compared to an arbitrary reference (Keeling and Shertz, 1992; Keeling et al., 2004) in per meg (one per meg is equal to 1×10^{-6}).

$$\delta(\mathrm{O_2/N_2}) = \frac{[n(\mathrm{O_2})/n(\mathrm{N_2})]_{\mathrm{sam}}}{[n(\mathrm{O_2})/n(\mathrm{N_2})]_{\mathrm{ref}}} - 1 \quad (1)$$

In the equation, *n* depicts the molar amount of each substance, and the subscripts sam and ref represent sample and reference air, respectively. The $\delta(O_2/N_2)$ value multiplied by 10^6 is expressed in per meg. The O_2 molar fraction in air in 2015 is 209339.1 ± 1.1 μmol mol^{-1} (Aoki et al., 2019). Therefore, adding 1 μmol of O_2 to a mole of dry air will increase in $\delta(O_2/N_2)$ by 4.8 per meg.

Each laboratory has typically employed its own O_2/N_2 reference based on natural air compressed and stored in high-pressure cylinders. Each laboratory has also assumed responsibility for calibrating the relationship between the measured instrument response and the reported change per meg units (span sensitivity). Therefore, the reported trends in O_2/N_2 are potentially biased

by any long-term drift in the O_2/N_2 ratio of the reference cylinders (zero drift) or errors in the calibrated span sensitivity of the instrument (span error). Note that a span stability below 5 per meg is required for the global CO_2 budget analyses based on $\delta(O_2/N_2)$ observations [Table 2 in Keeling et al. (1993)]. Challenges in achieving this stability include fractionations of O_2 and N_2 induced by pressure, temperature, and water vapour gradients (Keeling et al., 2007), adsorption/desorption of the constituents on the cylinder's inner surface (Leuenberger et al., 2015), and permeation/leakage of the constituents from/through the valve (Sturm et al., 2004; Keeling et al., 2007). Tohjima et al. (2005) developed high-precision O_2 standard mixtures with 2.9 μmol mol^{-1} uncertainty for O_2 molar fraction (equivalent to 15.5 per meg uncertainty for $\delta(O_2/N_2)$) in absolute terms to resolve these problems by preparing gravimetric standard mixtures of pure N_2, O_2, Ar, and CO_2. Their study was significant, but the uncertainty larger than those recommended by Keeling et al. (1993) still remains, as mentioned above.

Recently, a technique was developed for preparing high-precision primary standard mixtures with standard uncertainties less than 5 per meg for $\delta(O_2/N_2)$ at the National Metrology Institute of Japan, National Institute of Advanced Industrial Science and Technology (NMIJ/AIST) (Aoki et al., 2019). The high-precision standard mixtures allow us to evaluate span offset accurately and precisely. Absolute drift of scale zero offset is also able to be evaluated accurately and precisely by periodically comparing laboratory reference air with the high-precision standard mixtures, which are prepared every time each comparison.

In this study, we conducted intercomparison experiments to compare span sensitivities among the O_2/N_2 scales of the Research Institute for Environmental Management Technology, Advanced Industrial Science and Technology (EMRI/AIST), National Institute for Environmental Studies (NIES), Tohoku University (TU), and Scripps Institution of Oceanography (SIO) based on round-robin exercise for the laboratory measuring the developed high-precision standard mixtures in order. Following this, a regression analysis is applied to the intercomparison results to investigate the relationship between the individual laboratory O_2/N_2 scales. Results showed a slight but significant difference in the span sensitivities of the individual scales. Finally, we compare the atmospheric $\delta(O_2/N_2)$ values observed on the EMRI/AIST scale with those on the NIES scale for the air samples collected at Hateruma Island (HAT; 24°03'N, 123°49'E), Japan, using the relationship between the individual laboratory scales obtained in this study.

2. Experimental Procedures

2.1 NMIJ/AIST Scale and Round-robin Standard Mixtures

In this study, five high-precision standard mixtures with standard uncertainties less than 5 per meg for $\delta(O_2/N_2)$ were used as round-robin standard mixtures. The NMIJ/AIST previously mixed them gravimetrically following ISO 6142-1:2015 (Aoki et al., 2019). The gravimetric preparation technique's detail was given in previous papers (Aoki et al., 2019, Matsumoto et al., 2004, 2008). They were contained in 10 L aluminium-alloy cylinders (Luxfer Gas Cylinders, UK) with a diaphragm brass valve (G-55, Hamai Industries Limited, Japan). Table 1 shows the gravimetrically determined molar fractions for N_2, O_2, Ar, CO_2, as well as $\delta(O_2/N_2)$ in the round-robin standard mixtures. The gravimetric values of N_2, O_2, Ar, and CO_2 molar fractions

were recalculated based on the cylinders' updated expansion rate, which was used for the correction of buoyancy acting a cylinder. The updated rate was determined as 1.62 ± 0.06 ml Mpa^{-1} (unpublished data), which was determined by measuring change of water volume with depletion of inner pressure of the cylinders sunk in water since the previous expansion rate (2.2 ± 0.2 ml Mpa^{-1}) was provided by a cylinder supplier. The source gases used are pure CO_2 (>99.998%, Nippon Ekitan Corp., Japan), pure Ar (99.9999%, G1-grade, Japan Fine Products, Japan), pure O_2 (99.99995%, G1-grade, Japan Fine Products, Japan), and pure N_2 (99.99995%, G1-grade, Japan Fine Products, Japan). Impurities in the source gases were identified and quantified via several techniques. GC equipped with a thermal conductivity detector (GC/TCD) was used to analyse N_2, O_2, CH_4, and H_2 in pure CO_2. O_2 and Ar in pure N_2 and N_2 in pure O_2 were analysed using GC, equipped with a mass spectrometer. A Fourier-transform infrared spectrometer was used to detect CO_2, CH_4, and CO in pure N_2, O_2, and Ar. A galvanic cell O_2 analyser was used to quantify O_2 in pure Ar. A capacitance-type moisture sensor measured H_2O in pure CO_2, and a cavity ring-down moisture analyser measured H_2O in pure N_2, O_2, and Ar.

In this study, the absolute O_2/N_2 scale determined using the gravimetric values in the round-robin standard mixtures is hereafter called as the NMIJ/AIST scale. The NMIJ/AIST scale is presented only for scientific research and is uncertified by NMIJ. Here, $\delta(O_2/N_2)_{NMIJ/AIST}$ represents the $\delta(O_2/N_2)$ on the NMIJ/AIST scale. We arbitrarily assigned zero on the NMIJ/AIST scale to be a ratio of 0.2093391/ 0.7808943=0.2680761, which corresponded to atmospheric O_2/N_2 ratio 2015 (Aoki et al., 2019). The range of $\delta(O_2/N_2)_{NMIJ/AIST}$ values for the round-robin standard mixtures was −3600 per meg to 2900 per meg in order to evaluate the difference of the individual span sensitivities accurately although it is larger than their variation in air. The standard uncertainties of the $\delta(O_2/N_2)_{NMIJ/AIST}$ values were 3.3 per meg to 4.0 per meg.

2.2 Procedure of Intercomparison

The EMRI/AIST, NIES, TU, and SIO conducted the intercomparison experiment. Five round-robin standard mixtures were analysed in the order of EMRI/AIST (May to July 2017), NIES (September to November 2017), TU (December 2017 to January 2018), and SIO (May to December 2018). Each lab reported the $\delta(O_2/N_2)_{round\text{-}robin}$ values as determined against their scales to the NMIJ/AIST. The $\delta(O_2/N_2)_{round\text{-}robin}$ hereafter represents the $\delta(O_2/N_2)$ values measured by individual laboratories. Each lab analysed air delivered from the cylinders after placing them horizontally for more than five days after their transport to avoid the change of $\delta(O_2/N_2)$ values in the standard mixtures by thermal diffusion and gravitational fractionation. The $\delta(O_2/N_2)_{round\text{-}robin}$ values determined by the individual laboratories using their methods were compared with the $\delta(O_2/N_2)_{NMIJ/AIST}$ values. EMRI/AIST and TU used mass spectrometry, NIES used GC, and SIO used the interferometric method, as summarised in Table 2. The stability of O_2/N_2 ratios in the round-robin standard mixtures during the intercomparison experiment was evaluated by measuring their $\delta(O_2/N_2)_{round\text{-}robin}$ values using a mass spectrometer (Delta-V, Thermo Fisher Scientific Inc., USA) (Ishidoya and Murayama, 2014) at EMRI/AIST during the intercomparison experiment. Ar molar fractions in the round-robin standard mixtures were from 9297 to 9351 μmol mol^{-1}, much larger than variations in the tropospheric air (less than 1 μmol mol^{-1}) (Keeling et al., 2004). Isotopic ratios of $\delta(^{17}O/^{16}O)$, $\delta(^{18}O/^{16}O)$, and $\delta(^{15}N/^{14}N)$ in

the round-robin standard mixtures were determined by the mass spectrometer at EMRI/AIST to be 4.7‰, 9‰, and 2.4‰, larger than the atmosphere. The atmospheric value is used as primary standard (De Laeter et al., 2003, Wieser and Berglund, 2009). $\delta(^{17}O/^{16}O)$, $\delta(^{18}O/^{16}O)$, and $\delta(^{15}N/^{14}N)$ are expressed as

$$\delta\left(^{17}O/^{16}O\right) = \frac{\left[n(^{17}O)/n(^{16}O)\right]_{sam}}{\left[n(^{17}O)/n(^{16}O)\right]_{ref}} - 1 \quad (2)$$

$$\delta\left(^{18}O/^{16}O\right) = \frac{\left[n(^{18}O)/n(^{16}O)\right]_{sam}}{\left[n(^{18}O)/n(^{16}O)\right]_{ref}} - 1 \quad (3)$$

$$\delta\left(^{15}N/^{14}N\right) = \frac{\left[n(^{15}N)/n(^{14}N)\right]_{sam}}{\left[n(^{15}N)/n(^{14}N)\right]_{ref}} - 1. \quad (4)$$

Here, the isotopic ratios of $\delta(^{17}O/^{16}O)$, $\delta(^{18}O/^{16}O)$, and $\delta(^{15}N/^{14}N)$ were approximately equal to those of $\delta(^{17}O^{16}O/^{16}O^{16}O)$, $\delta(^{18}O^{16}O/^{16}O^{16}O)$, and $\delta(^{15}N^{14}N/^{14}N^{14}N)$. This is because $^{17}O^{17}O/^{16}O^{16}O$, $^{18}O^{18}O/^{16}O^{16}O$, and $^{15}N^{15}N/^{14}N^{14}N$ tended to be lower than $^{17}O^{16}O/^{16}O^{16}O$, $^{18}O^{16}O/^{16}O^{16}O$, and $^{15}N^{14}N/^{14}N^{14}N$ by 5000 times, 1000 times, and 500 times, respectively, which were roughly calculated based on the abundances of $^{17}O^{17}O$ and $^{17}O^{16}O$, $^{18}O^{18}O$ and $^{18}O^{16}O$, and $^{15}N^{15}N$ and $^{15}N^{14}N$.

Values of $\delta(O_2/N_2)$ in sample air have generally been determined on assumption that Ar molar fractions and isotopic ratios of N_2 and O_2 in reference air and sample air are identical. However, the round-robin standard mixtures had different in the Ar molar fraction and the isotopic ratios from reference air. We applied the following corrections to the measured $\delta(O_2/N_2)_{round\text{-}robin}$ values from the individual laboratories by considering the deviations in the Ar molar fraction and the isotopic ratios in the round-robin standard mixtures from the atmospheric level. The $\delta(O_2/N_2)_{round\text{-}robin}$ values reported by EMRI/AIST and TU were corrected based on the deviation in the isotope ratio from the atmospheric level using isotopic ratios of N_2 and O_2 measured simultaneously at EMRI/AIST. This is because EMRI/AIST and TU measured the values of $\delta(^{16}O^{16}O/^{14}N^{14}N)$ and $\delta(^{16}O^{16}O/^{14}N^{15}N)$, respectively. NIES corrected $\delta(O_2/N_2)_{round\text{-}robin}$ using the Ar molar fraction difference from its atmospheric level since the O_2 peak obtained in GC included the Ar peak. SIO also corrected $\delta(O_2/N_2)_{round\text{-}robin}$ using the difference in the Ar molar fraction from its atmospheric level since they only measured O_2 molar fractions. The measurement techniques and calculation procedures of the $\delta(O_2/N_2)_{round\text{-}robin}$ values for individual laboratories are detailed in the next section.

2.3 Analytical and Calculation Methods of $\delta(O_2/N_2)$ Values

2.3.1 EMRI/AIST

The $\delta(O_2/N_2)_{round\text{-}robin}$ values for EMRI/AIST were calculated based on the $\delta(^{16}O^{16}O/^{14}N^{14}N)_{round\text{-}robin}$ values measured using the mass spectrometer. The $\delta(^{16}O^{16}O/^{14}N^{14}N)_{round\text{-}robin}$ values were calculated against the reference air on the EMRI/AIST scale, which is natural air filled in a 48 L aluminium cylinder with a diaphragm valve (G-55, Hamai Industries Limited, Japan). The EMRI/AIST scale's long-term stability is described in following section 3.1. The measurement technique's detail was given in Ishidoya and Murayama (2014). The mass spectrometer was adjusted to measure ion beam currents for masses 28 ($^{14}N^{14}N$), 29 ($^{15}N^{14}N$), 32 ($^{16}O^{16}O$), 33 ($^{17}O^{16}O$), 34 ($^{18}O^{16}O$), and 44 ($^{12}C^{16}O^{16}O$). The $\delta(O_2/N_2)_{NMIJ/AIST}$ comprising all isotopes of N_2

and O_2 are not equivalent to the isotopic ratios of $\delta(^{16}O^{16}O/^{14}N^{14}N)_{round\text{-}robin}$ measured using the mass spectrometer since the isotope ratios of N_2 and O_2 in the round-robin standard mixtures are different from those in the reference air. Thus, mass-spectrometry-based isotopic ratios must be converted to values equivalent to the $\delta(O_2/N_2)_{NMIJ/AIST}$ values. The $\delta(O_2/N_2)_{round\text{-}robin}$ values were corrected based on isotopic ratios $^{15}N^{14}N/^{14}N^{14}N$, $^{17}O^{16}O/^{16}O^{16}O$, and $^{18}O^{16}O/^{16}O^{16}O$ in the round-robin standard mixtures and reference air, as shown in Eq. (5).

$$\delta(O_2/N_2)_{round-robin} = \left[\delta(^{16}O^{16}O/\,^{14}N\,^{14}N) + 1\right]_{round-robin} \times \left[\frac{1+^{17}O^{16}O/^{16}O^{16}O+^{18}O^{16}O/^{16}O^{16}O}{1+^{15}N\,^{14}N/^{14}N^{14}N}\right]_{round-robin} \Big/ \left[\frac{1+^{17}O^{16}O/^{16}O^{16}O+^{18}O^{16}O/^{16}O^{16}O}{1+^{15}N\,^{14}N/^{14}N\,^{14}N}\right]_{ref} - 1. \quad (5)$$

Here, isotopic species of $^{17}O^{17}O$, $^{18}O^{17}O$, $^{18}O^{18}O$, and $^{15}N^{15}N$ were negligible since their abundance was sufficiently smaller than those of $^{17}O^{16}O$, $^{18}O^{16}O$, and $^{15}N^{15}N$. The isotopic ratios of $^{15}N^{14}N/^{14}N^{14}N$, $^{17}O^{16}O/^{16}O^{16}O$, and $^{18}O^{16}O/^{16}O^{16}O$ in the round-robin standard mixtures were calculated using Eqs. (6), (7), and (8).

$$^{18}O^{16}O/^{16}O^{16}O = [\delta(^{18}O^{16}O/^{16}O^{16}O)_{round\text{-}robin} + 1] \times (^{18}O^{16}O/^{16}O^{16}O)_{ref}, \quad (6)$$

$$^{17}O^{16}O/^{16}O^{16}O = [\delta(^{17}O^{16}O/^{16}O^{16}O)_{round\text{-}robin} + 1] \times (^{17}O^{16}O/^{16}O^{16}O)_{ref}, \quad (7)$$

$$^{15}N^{14}N/^{14}N^{14}N = [\delta(^{15}N^{14}N/^{14}N^{14}N)_{round\text{-}robin} + 1] \times (^{15}N^{14}N/^{14}N^{14}N)_{ref}. \quad (8)$$

The isotopic ratios of $\delta(^{17}O^{16}O/^{16}O^{16}O)_{round\text{-}robin}$, $\delta(^{18}O^{16}O/^{16}O^{16}O)_{round\text{-}robin}$, and $\delta(^{15}N^{14}N/^{14}N^{14}N)_{round\text{-}robin}$ were determined to be 4.7‰, 9‰, and 2.4‰ against the EMRI/AIST reference air as mentioned above. Values of $(^{18}O^{16}O/^{16}O^{16}O)_{ref}$, $(^{17}O^{16}O/^{16}O^{16}O)_{ref}$, and $(^{15}N^{14}N/^{14}N^{14}N)_{ref}$ refer to ratios of $^{18}O^{16}O/^{16}O^{16}O$, $^{17}O^{16}O/^{16}O^{16}O$, and $^{15}N^{14}N/^{14}N^{14}N$ in the reference air. We regard the isotopic ratios in the EMRI/AIST reference air as atmospheric values since differences between N_2, O_2, and Ar in the AIST reference air and air samples at Hateruma were small enough to be negligible. Therefore, the corresponding atmospheric values were used to calculate the ratios of $(^{18}O^{16}O/^{16}O^{16}O)_{ref}$, $(^{17}O^{16}O/^{16}O^{16}O)_{ref}$, and $(^{15}N^{14}N/^{14}N^{14}N)_{ref}$, which can be taken as globally constant because atmospheric mixing is very rapid compared to the processes altering oxygen isotopic composition (Junk and Svec, 1958; Baertschi, 1976; Li et al., 1988; Barkan and Luz, 2005).

2.3.2 NIES

NIES reported the $\delta(O_2/N_2)_{round\text{-}robin}$ values based on the $\delta\{(O_2+Ar)/N_2\}_{round\text{-}robin}$ values measured using a GC/TCD (Tohjima, 2000). The $\delta\{(O_2+Ar)/N_2\}_{round\text{-}robin}$ values were calculated against the reference air on the NIES scale, which is natural air filled in a 48 L aluminium cylinder. A column separates the (O_2 + Ar) and N_2 in the air sample, and a TCD detected the

individual peaks. The reference and sample air were repeatedly measured using the GC/TCD, and the $\delta\{(O_2+Ar)/N_2\}_{\text{round-robin}}$ values were calculated based on the ratios of the (O_2 + Ar) peak area to N_2 peak area using Eq. (9).

$$\delta\{(O_2 + Ar)/N_2\}_{\text{round-robin}} = \frac{\{(O_2+kAr)/N_2\}_{\text{round-robin}}}{\{(O_2+kAr)/N_2\}_{\text{ref}}} - 1. \quad (9)$$

The $\delta(O_2/N_2)_{\text{round-robin}}$ value is given by Eq. (10).

$$\delta(O_2/N_2)_{\text{round-robin}} = (1 + a) \times \delta\{(O_2 + Ar)/N_2\}_{\text{round-robin}} - a \times \delta(Ar/N_2)_{\text{round-robin}}, \quad (10)$$

where the coefficient a is defined by $a = k(Ar/O_2)_{\text{ref}}$. k represents the TCD sensitivity ratio of Ar relative to O_2, and the value was evaluated as 1.13 by comparing gravimetric mixtures of O_2 + N_2 and Ar + O_2 + N_2 (Tohjima et al., 2005). Natural air is used for the reference air. Therefore, the value of a is calculated as 0.050 (Ar = 0.93% and O_2 = 20.94%). For NIES, the $\delta(Ar/N_2)_{\text{round-robin}}$ value was calculated using the gravimetric values of N_2 and Ar in the round-robin standard mixtures.

The NIES O_2/N_2 scale is related to a set of 11 primary reference air cylinders. The NIES O_2/N_2 scale's long-term stability has been maintained within ±0.45 per meg yr^{-1} with respect to these cylinders by analysing the relative differences in the O_2/N_2 ratios in the primary and working reference air (Tohjima et al., 2019). Details of the analytical methods and the NIES O_2/N_2 scale are given in Tohjima et al. (2005, 2008).

2.3.3 TU

The $\delta(O_2/N_2)_{\text{round-robin}}$ values for TU were calculated based on the $\delta(^{16}O^{16}O/^{15}N^{14}N)_{\text{round-robin}}$ values measured using a mass spectrometer (Finnigan MAT-252). The $\delta(^{16}O^{16}O/^{15}N^{14}N)_{\text{round-robin}}$ values were calculated against the reference air on the TU scale, which is natural air filled in a 47 L manganese steel cylinder in 1998. The measurement technique's detail was given by Ishidoya et al. (2003). The TU scale's stability was evaluated by measuring the values of $\delta(O_2/N_2)$ in six working reference air against the primary reference air from 1999 to 2020. The changing rate and their standard deviation of $\delta(O_2/N_2)$ in the working reference air were −0.02 ± 0.37 per meg yr^{-1} on average. The mass spectrometer was adjusted to measure ion beam currents for masses 29 ($^{15}N^{14}N$) and 32 ($^{16}O^{16}O$), because the spread of both ion beams for mass 28 and 32 was too wide to measure simultaneously. The $\delta(O_2/N_2)_{\text{NMIJ/AIST}}$ values are not equivalent to the isotopic ratios of $\delta(^{16}O^{16}O/^{15}N^{14}N)_{\text{round-robin}}$ measured by TU as above described reason. Therefore, the $\delta(O_2/N_2)_{\text{round-robin}}$ values were calculated using the isotopic ratios $^{14}N^{14}N/^{15}N^{14}N$, $^{17}O^{16}O/^{16}O^{16}O$, and $^{18}O^{16}O/^{16}O^{16}O$, as shown in Eq. (11).

$$\delta(O_2/N_2)_{\text{round-robin}} = \left[\delta(^{16}O^{16}O/\,^{15}N\,^{14}N) + 1\right]_{\text{round-robin}} \times \left[\frac{1+^{17}O^{16}O/^{16}O^{16}O+^{18}O^{16}O/^{16}O^{16}O}{1+^{14}N\,^{14}N/^{15}N^{14}N}\right]_{\text{round-robin}} \Big/ \left[\frac{1+^{17}O^{16}O/^{16}O^{16}O+^{18}O^{16}O/^{16}O^{16}O}{1+^{14}N\,^{14}N/^{15}N^{14}N}\right]_{\text{ref}} - 1 \quad (11)$$

The isotopic ratios in the round-robin standard mixtures were calculated using Eqs. (6), (7), and (12).

$$^{14}N^{14}N/^{15}N^{14}N = [\delta(^{14}N^{14}N/^{15}N^{14}N)_{\text{round-robin}} + 1] \times (^{14}N^{14}N/^{15}N^{14}N)_{\text{ref}}. \quad (12)$$

In this study, we used the values of $\delta(^{18}O^{16}O/^{16}O^{16}O)_{\text{round-robin}}$, $\delta(^{17}O^{16}O/^{16}O^{16}O)_{\text{round-robin}}$, and $\delta(^{14}N^{14}N/^{15}N^{14}N)_{\text{round-robin}}$ measured by EMRI/AIST, rather than by TU, to reduce the uncertainties of the $\delta(O_2/N_2)_{\text{round-robin}}$ values associated with the isotope ratio measurements. The $(^{18}O^{16}O/^{16}O^{16}O)_{\text{ref}}$, $(^{17}O^{16}O/^{16}O^{16}O)_{\text{ref}}$, and $(^{15}N^{14}N/^{14}N^{14}N)_{\text{ref}}$ values were calculated based on the corresponding atmospheric values, similar to the EMRI/AIST values.

2.3.4 SIO

SIO reported the $\delta(O_2/N_2)$ values based on measurements using a two-wavelength interferometer (Keeling et al., 1998). The SIO O_2/N_2 reference, of which scale is defined as $\delta(O_2/N_2) = 0$, is based on a suite of 18 primary reference gases stored in high-pressure cylinders (aluminium or steel, volumes ranging from 29 to 47 L) filled with natural air (Keeling et al., 2007). The SIO O_2/N_2 scale's long-term stability has been maintained within ±0.4 per meg yr^{-1} with respect to these cylinders by analysing the relative differences in the O_2/N_2 ratios in the primary reference air. Differences between the round-robin cylinders and the SIO reference were determined from

$$\delta(O_2/N_2)_{\text{round-robin}} = \frac{1}{S_{O_2} \cdot X_{O_2}(1-X_{O_2})} \cdot \delta\tilde{r} - I_{CO_2} \cdot \Delta CO_2 - I_{Ar/N_2} \cdot \delta(Ar/N_2) - other\ interferences \quad (13)$$

where $\delta\tilde{r}$ is the difference in refractivity ratio $\tilde{r}$ = r(2537.27 Å)/r(4359.57 Å) between the round-robin cylinder and the SIO reference, determined via interferometric comparisons with secondary reference gases linked to the primary suite. S_{O_2} =0.03397 is a constant sensitivity factor, X_{O_2} is the molar fraction of the SIO reference, I_{CO_2} is a constant (1.0919 per meg/ppm), and ΔCO_2 is the difference in CO_2 molar fraction from the SIO reference (363.29 μmol mol^{-1}). SIO data are routinely corrected for CO_2 interference. The sensitivity S_{O_2} and interference factors (e.g., I_{Ar/N_2} = −0.0124) in Eq. (13) are based on refractivity data for the pure gases and natural air (Keeling, 1988b, Keeling et al., 1998). SIO applies additional corrections for Ar/N_2, Ne, He, Kr, Xe, CH_4, N_2O, and CO. The additional corrections are effectively constant (or small) in natural air. They can usually be neglected in comparisons of natural air samples. However, these corrections cannot be neglected in relating the SIO scale to an absolute O_2/N_2 reference based on the round-robin cylinders, which differ in their Ar/N_2 ratios from natural air and which lack constituents other than N_2, O_2, Ar, and CO_2. These corrections require estimates of the molar Ar/N_2 ratio and other gases' abundances in typical background air. Notably, the primary reference gases are relevant in Eq. (13) as references for relative refractivity. Therefore, the exact Ar/N_2 ratio and abundances of other gases in

the SIO reference are not directly relevant. For background air, the following values were adopted: Ar/N_2 = 0.0119543, Ne/N_2 = 2.328×10^{-5}, He/N_2 = 6.71×10^{-6}, Kr/N_2 = 1.46×10^{-6}, Xe/N_2 = 1.11×10^{-7}, CH_4 = 1.8 μmol mol^{-1}, N_2O = 0.3 μmol mol^{-1}, CO = 0.1 μmol mol^{-1}. Here, Ar/N_2 is from Aoki et al. (2019), and the other (noble gas)/N_2 ratios are from Glueckhauf (1951). using Xe data from Kronjäger (1936) (also see Keeling et al., 2020). The quantity $\delta(Ar/N_2)$ was computed using the AIST gravimetric data, $\delta(Ar/N_2) = ((Ar/N_2)_{grav}/0.0119543 - 1)$.

The Ar/N_2 interference ($-I_{Ar/N_2} \cdot \delta(Ar/N_2)$) ranges from −55 to + 24 per meg, depending on the round-robin cylinder. The sum of the remaining interferences, other than for CO_2 (- *other interferences*), is effectively constant at −14.3 per meg. The largest individual contributions are from Ne (−32.8 per meg) and CH_4 (+11.9 per meg).

3 Results and Discussion

3.1 Stability of $\delta(O_2/N_2)$ During Intercomparison

The $\delta(O_2/N_2)_{round\text{-}robin}$ values were measured four times using the mass spectrometer by EMRI/AIST to evaluate the stability of the O_2/N_2 ratios of the standard mixtures during the intercomparison experiment. The initial $\delta(O_2/N_2)_{round\text{-}robin}$ values in the measurement of four times were used as the EMRI/AIST assigned values. The $\delta(O_2/N_2)_{round\text{-}robin}$ values were calculated against the EMRI/AIST scale. The EMRI/AIST scale's stability was evaluated by measuring the values of $\delta(O_2/N_2)$ in three working reference air against the primary reference air from 2012 to 2020. The changing rate and their standard deviation of $\delta(O_2/N_2)$ in the respective cylinders were 0.08 ± 0.11 per meg yr^{-1} on average. Therefore, the working standards show no systematic trend in $\delta(O_2/N_2)$ regarding the primary reference air.

Figure 1 shows the temporal drifts of the $\delta(O_2/N_2)_{round\text{-}robin}$ values from the initial values determined by the mass spectrometer at EMRI/AIST. The first measurement was conducted immediately after preparing the round-robin standard mixtures: May 2017 for three cylinders (CPB16345, CPB16315, CPB16379) and July 2017 for the other cylinders (CPB28912, CPB16349). The temporal drifts analysed in March 2018 (before shipment) ranged from −5.9 to 5.5 per meg. This range was within the expanded uncertainty (6.4 per meg) of the measurement which was estimated based on standard uncertainty of $\delta(O_2/N_2)$ value measured using the mass spectrometer of EMRI/AIST. Here the expanded uncertainty (a coverage factor of 2) represents ≈ a 95% level of confidence. The temporal drifts analysed in March 2019 (after the cylinders' return from SIO) ranged from −16.4 per meg to 2.9 per meg. This range was larger than the expanded uncertainty of the measurement.

We also analysed the round-robin standard mixtures in March 2020 (a year after return) and found that the temporal drifts ranged from −18.3 per meg to −5.6 per meg. The $\delta(O_2/N_2)_{round\text{-}robin}$ values decreased with time in all cylinders, especially for cylinder no. CPB16379. The average decreasing rate of the $\delta(O_2/N_2)_{round\text{-}robin}$ values in the cylinders, except for CPB16379, was −3.2 ± 1.1 per meg yr^{-1}. Meanwhile, that of the CPB16379 cylinder was −6.7 ± 2.1 per meg yr^{-1}. The decreasing rates and standard deviations were calculated from least-square fitting. The decrease in the $\delta(O_2/N_2)_{round\text{-}robin}$ values during the

intercomparison experiment are thought to be caused by O_2 consumption by the oxidation of residual organic material, oxidation of the inner surface of the cylinders, and the difference in adsorption/desorption between N_2 and O_2 on the inner surface of the cylinders rather than the fractionation of N_2 and O_2 since the escape of gas from the cylinder generally increases the O_2/N_2 in a cylinder (Langenfelds et al., 1999). We corrected the temporal drifts during the intercomparison experiment by linearly interpolating the $\delta(O_2/N_2)_{NMIJ/AIST}$ value of the date analysed by individual laboratories using the temporal drifts measured before and after the analysis of individual laboratories. The correction was performed in each cylinder separately. Following this, we compared the interpolated $\delta(O_2/N_2)_{NMIJ/AIST}$ value with the measured $\delta(O_2/N_2)_{round\text{-}robin}$ value.

We evaluated the NMIJ/AIST scale's reproducibility at EMRI/AIST using nine high-precision standard mixtures prepared in different periods (from April 2017 to February 2020). Figure 2 shows the relations between the $\delta(O_2/N_2)_{NMIJ/AIST}$ values gravimetrically determined by NMIJ/AIST and the $\delta(O_2/N_2)$ values measured using the mass spectrometer at EMRI/AIST. The lines in Figure 2a represent the Deming least-square fit to the data, and Figure 2b shows residuals of $\delta(O_2/N_2)_{NMIJ/AIST}$ from the line. The error bar represents the expanded uncertainty of the $\delta(O_2/N_2)_{NMIJ/AIST}$ values. All residuals were within the expanded uncertainties of less than 8 per meg, which showed that the NMIJ/AIST scale could be reproduced any time by preparing high-precision standard mixtures. This show that an absolute long-term temporal stability of each laboratory's $\delta(O_2/N_2)$ scale, which is determined against a reference natural air in a high-pressure cylinder, can be evaluated by comparing the reference air with high-precision standard mixtures prepared by NMIJ/AIST at interval.

3.2 Intercomparison Between Laboratory Scales and Their Span Sensitivities

Table 3 summarises the $\delta(O_2/N_2)_{round\text{-}robin}$ values measured by individual laboratories. Notably, $\delta(O_2/N_2)_{round\text{-}robin}$ values shown in Table 3 are corrected for the deviations in Ar/N_2 ratios and isotopic ratios of N_2 and O_2 in the round-robin standard mixtures from the atmospheric values and determined against their scales, as described in Section 2.3.

Figure 3a represents the relations between the $\delta(O_2/N_2)_{NMIJ/AIST}$ and $\delta(O_2/N_2)_{round\text{-}robin}$ values of individual laboratories. The $\delta(O_2/N_2)_{NMIJ/AIST}$ values were interpolated to correct the temporal drifts of $\delta(O_2/N_2)$, as described in Section 3.1. The lines represent a Deming least-square fit to the plotted data for individual laboratories. The slopes and their standard uncertainty for EMRI/AIST, TU, NIES, and SIO were 0.9989 ± 0.0010, 0.9990 ± 0.0013, 1.0339 ± 0.0013, and 1.0093 ± 0.0010, respectively (Table 4). The deviations from 1 for the slopes of the lines represent the differences from the NMIJ/AIST scale's span sensitivity, of which their relative values were −0.11 ± 0.10, −0.10 ± 0.13, 3.39 ± 0.13, and 0.93 ± 0.10 % for EMRI/AIST, TU, NIES, and SIO, respectively. The intercepts of the lines represent the differences between individual laboratory scales and the NMIJ/AIST scale corresponding to $\delta(O_2/N_2)_{NMIJ/AIST} = 0$: 65.8 ± 2.2, 425.7 ± 3.1, 404.5 ± 3.0, and 596.4 ± 2.4 per meg for EMRI/AIST, TU, NIES, and SIO, respectively. The numbers following the symbol ± represent the standard uncertainties which were calculated based on the Deming least-square fit. The differences in intercepts between individual scales reflect those of O_2 mole fractions in the laboratory's reference air.

The differences in the intercepts between SIO and other laboratories were −530.6 ± 3.3, −170.8 ± 3.9, and −191.9 ± 3.9 per meg for EMRI/AIST, TU, and NIES, respectively. The differences of NIES and TU from SIO were consistent with those obtained from a past intercomparison experiment, which is the GOLLUM exercise coordinated by SIO and the University of East Anglia from 2003-2014 (GOLLUM, 2015, WMO, 2003, and A. Manning personal communication), within their uncertainties (Table 4). Figure 3b shows the residuals from the fitting lines. The error bar represents the expanded uncertainty which was calculated based on the standard uncertainties of $\delta(O_2/N_2)$ values measured by individual laboratories. All of them fall within expanded uncertainties.

3.3 Compatibility of the Atmospheric $\delta(O_2/N_2)$ Data Between the Laboratories and Its Implication to the Global CO_2 Budget Analysis

This study aims that the intercomparison results allow us to compare the observation data of individual laboratories directly. We compared the O_2/N_2 ratios measured by EMRI/AIST and NIES based on flask samples collected at HAT from October 2015 to December 2019 (Tohjima et al., 2008). The values of NIES after March 2018 are preliminary data. The air samples were collected twice monthly into two Pyrex glass flasks arranged in series (one for AIST and the other for NIES). We confirmed that the isotopic ratios of N_2 and O_2 in the reference air of EMRI/AIST and NIES did not significantly differ from the atmospheric values for the HAT air samples. The $\delta(^{15}N^{14}N/^{14}N^{14}N)$ and $\delta(^{18}O^{16}O/^{16}O^{16}O)$ values in the air samples were in range from 0 per meg to 10 per meg on the EMRI/AIST scale, suggesting that the difference in isotopic ratios of N_2 and O_2 between the air samples and the reference air of the EMRI/AIST scale was significantly small. Therefore, we regard the values of $\delta(^{16}O^{16}O/^{14}N^{14}N)$ and $\delta\{(O_2+Ar)/N_2\}$ which were measured using the mass spectrometer and GC/TCD equal to $\delta(O_2/N_2)$ in Eq. (1). Figure 4a shows the $\delta(O_2/N_2)$ values reported on the NIES and EMRI/AIST scales. The average difference in the $\delta(O_2/N_2)$ between the two scales was −329.3 ± 6.9 per meg (subtracting the $\delta(O_2/N_2)$ values of EMRI/AIST from those of NIES). The uncertainty represents the standard deviation of the differences. Both values of $\delta(O_2/N_2)$ were converted to the NMIJ/AIST scale using Eq. (14),

$$\delta(O_2/N_2)_{\mathrm{NMIJ/AIST}} = a_n \cdot \delta(O_2/N_2)_n + b_n, \tag{14}$$

where a_n and b_n are the slope and intercept of each laboratory's line (n) obtained in Section 3.2. Figure 4b shows the converted $\delta(O_2/N_2)$ values. The average difference and the standard deviation in the converted $\delta(O_2/N_2)$ between the two scales was −6.6 ± 6.8 per meg, which showed that this scale conversion reduced the bias between the $\delta(O_2/N_2)$ values of EMRI/AIST and NIES. The bias dropped within the standard deviation, although it was more than the compatibility goal of 5 per meg for the O_2/N_2 ratio measurement. Figures 5a and 5b plot both values of $\delta(O_2/N_2)$ before and after the scale conversion, confirming the compatibility between the span sensitivities on the EMRI/AIST and NIES scales. The lines represent a Deming least-square fit to the scatter plots. The slope of the line before scale conversion and its standard uncertainty are 0.956 ± 0.015, consistent

with the difference in the span sensitivity between both scales (0.9989/1.0339 = 0.966) within uncertainty. After the scale conversion, the slope and its standard uncertainty are 0.990 ± 0.015, identifying that the scale conversion improved the difference in the span sensitivity between the EMRI/AIST and NIES scales to the NMIJ/AIST scales.

Observing the long-term trend in atmospheric $\delta(O_2/N_2)$ provides critical information on the global CO_2 budget (Manning and Keeling, 2006). Recently, Tohjima et al. (2019) estimated the land biospheric and oceanic CO_2 uptakes using the average changing rate of atmospheric O_2/N_2 ratio and CO_2 molar fraction reported on the NIES scale. We converted the changing rate of $\delta(O_2/N_2)$ on the NIES scale to that on the NMIJ/AIST scales and recalculated the global CO_2 budgets from 2000 to 2016 using the converted rates. Table 5 summarises the CO_2 budgets reported by Tohjima et al. (2019) and recalculated by this study. Notably, the fossil fuel-derived CO_2 emissions and the global average of the atmospheric CO_2 molar fractions used for the CO_2 budget calculation are the same as those used in the Global Carbon Project for estimating the global carbon budget in 2020 (Friedlingstein et al., 2020).

We found a decrease and increase of 0.30 Pg yr^{-1} to the land biospheric and oceanic CO_2 uptakes due to the scale conversions as shown in Table 5. These amounts correspond to 20% and 12% of the land biospheric and oceanic carbon budgets estimated by NIES and are not negligible. Results show that the span sensitivities of the O_2/N_2 scale are critical to accurately estimating carbon budgets. Moreover, Resplandy et al. (2019) estimated an increase in the global ocean heat content (OHC) based on atmospheric O_2 and CO_2 measurements. They reported that the largest single source of uncertainty in their estimation is the scale error from the span calibration of the O_2/N_2 analyser which is 2% on $\delta(O_2/N_2)$ contribution. They also mentioned that the error would be reduced via within-lab and inter-lab comparisons. Therefore, if the scale error is corrected using the span offset and the standard uncertainty of SIO scales against the NMIJ/AIST absolute scale obtained from the intercomparison experiment, the scale error may reduce from 2 % to 0.1 %, which should improve the accuracy of the OHC increase estimate significantly.

4 Conclusions

The intercomparison experiment was used to evaluate the relationship between the measured $\delta(O_2/N_2)$ values and span sensitivities of the individual laboratory scales from the NMIJ/AIST scale using gravimetrically prepared high-precision standard mixtures. The relative deviations in span sensitivity of the EMRI/AIST, TU, NIES, and SIO scales against the NMIJ/AIST scale were −0.11 ± 0.10, −0.10 ± 0.13, 3.39 ± 0.13, and 0.93 ± 0.10 %, which were quantified for the first time in the world. The largest offset corresponded to the 0.30 Pg yr^{-1} decrease and increase in global estimates for land biospheric and oceanic CO_2 uptakes, which are not negligible. The deviations in the measured $\delta(O_2/N_2)$ values on the EMRI/AIST, TU, NIES, and SIO scales from the NMIJ/AIST scale corresponding to $\delta(O_2/N_2)_{NMIJ/AIST} = 0$ were 65.8 ± 2.2, 425.7 ± 3.1, 404.5 ± 3.0, and 596.4 ± 2.4 per meg, respectively. The differences between individual absolute values were consistent with the results from the GOLLUM round-robin cylinder comparison. However, the $\delta(O_2/N_2)$ values in the five round-robin standard mixtures decreased at rates of −6.7 ± 2.1 per meg yr^{-1} for one cylinder and −3.2 ± 1.1 per meg yr^{-1} for the other four cylinders. The

decrease suggests that it is necessary to evaluate long-term stability of laboratory's scale absolutely to link future $\delta(O_2/N_2)$ values. The O_2/N_2 ratios in high-precision standard mixtures prepared in different periods by NMIJ/AIST are reproduced within the O_2/N_2 ratios' uncertainty, identifying that the NMIJ/AIST scale can be reproduced any time by preparing high-precision standard mixtures. Further, a long-term temporal drift of each laboratory's scale can be evaluated by comparing the reference air with high-precision standard mixtures prepared by NMIJ/AIST. Finally, we demonstrated that the differences between $\delta(O_2/N_2)$ on the EMRI/AIST and NIES scales in flask samples collected at HAT became consistent within uncertainty by converting both scales to the NMIJ/AIST scale, although the bias of -6.6 ± 6.8 per meg is not negligible. The results obtained in this study should improve the estimation method of carbon budgets and OHC increase through more precise estimation of atmospheric $\delta(O_2/N_2)$ trend. The span sensitivities of the laboratory O_2/N_2 scales will be able to be absolutely evaluated by calibrating the cylinders based on the NMIJ/AIST scale if the GOLLUM will be performed using cylinders with sufficient different O_2/N_2 ratios. We expect that the compatibility goal of 5 per meg for the O_2/N_2 measurement is accomplished by comparing individual laboratory scale with absolute scale such as NMIJ/AIST scale.

Acknowledgments

We thank the Global Environmental Forum (GEF) staff for their work in collecting the air samples at the Hateruma station and Andrew Manning of the University of East Anglia coordinated the GOLLUM cylinder comparison programme and support the data acquisitions. Our research has been financially supported by the Global Environmental Research Coordination System from Ministry of the Environment of Japan (METI1454, METI1953) and the JSPS KAKENHI Grant Number 19K05554.

References

Aoki, N. and Shimosaka, T.: Development of an analytical system based on a paramagnetic oxygen analyzer for atmospheric oxygen variations, Anal. Sci., 34, 487–493, https://doi.org/10.2116/analsci.17P380, 2018.

Aoki, N., Ishidoya, S., Matsumoto, N., Watanabe, T., Shimosaka, T., and Murayama, S.: Preparation of primary standard mixtures for atmospheric oxygen measurements with less than 1 μmol mol^{-1} uncertainty for oxygen molar fractions, Atmos. Meas. Tech., 12, 2631–2626, https://doi.org/10.5194/amt-12-2631-2019, 2019.

Baertschi, P.: Absolute ^{18}O content of standard mean ocean water, Earth Planet. Sci. Lett., 31, 341–344, https://doi.org/10.1016/0012-821X(76)90115-1, 1976.

Barkan, E. and Luz, B.: High precision measurements of $^{17}O/^{16}O$ and $^{18}O/^{16}O$ ratios in H_2O, Rapid Commun. Mass Spectrom., 19, 3737–3742, https://doi.org/10.1002/rcm.2250, 2005.

Bender, M. L., Tans, P. P., Ellis, J. T., Orchard, J., and Habfast, K.: High precision isotope ratio mass spectrometry method for measuring the O_2/N_2 ratio of air, Geochim. Cosmochim. Acta., 58, 4751–4758, https://doi.org/10.1002/(SICI)1096-9888(199603)31:3<225::AID-JMS319>3.0.CO;2-L, 1994.

Bender, M. L., Ho, D. T., Hendricks, M. B., Mika, R., Battle, M. O., Tans, P. P., Conway, T. J., Sturtevant, B., and Casser, N.: Atmospheric O_2/N_2 changes,1993-2002: Implications for the partitioning of fossil fuel CO_2 sequestration, Global Biogeochem. Cy., 19, GB4017, https://doi.org/10.1029/2004GB002410, 2005.

Berhanu, T. A., Hoffnagle, J., Rella, C., Kimhak, D., Nyfeler, P., and Leuenberger, M.: High-precision atmospheric oxygen measurement comparisons between a newly built CRDS analyzer and existing measurement techniques, Atmos. Meas. Tech., 12, 6803–6826, https://doi.org/10.5194/amt-12-6803-2019, 2019

De Laeter, J. R., Böhlke, J. K., De Bièfre, P., Hidaka, H., Peiser, H. S., Rosman, K. J. R., & 5 Taylor P. D. P. (2003),Atomic weights of the elements: Review 2000 (IUPAC Technical Report), Pure Appl. Chem., 75, 683–800.

Friedlingstein, P., O'Sullivan, M., Jones, M. W., Andrew, R. M., Hauck, J., Olsen, A., Peters, G. P., Peters, W., Pongratz, J., Sitch, S., Le Quéré, C., Canadell, J. G., Ciais, P., Jackson1, R. B., Alin, S., Aragão, L. E. O. C., Arneth, A., Arora, V., R. Bates, N., Becker, M., Benoit-Cattin, A., Bittig, H. C., Bopp, L., Bultan, S., Chandra, N., Chevallier, F., Chini, L. P., Evans, W., Florentie, L., Forster, P. M., Gasser, T., Gehlen, M., Gilfillan, D., Gkritzalis, T., Gregor, L., Gruber, N., Harris, I., Hartung, K., Haverd, V., Houghton, R. A., Ilyina, Ta., Jain, A. K., Joetzjer, E., Kadono, K., Kato, E., Kitidis, V., Korsbakken, J. I., Landschützer, P., Lefèvre, N., Lenton, A., Lienert, S., Liu, Z., Lombardozzi, D., Marland, G., Metzl, N., Munro, D. R., Nabel, J. E. M. S., Nakaoka, S., Niwa, Y., O'Brien, K., Ono, T., Palmer, P. I., Pierrot, D., Poulter, B., Resplandy, L., Robertson, E., Rödenbeck, C., Schwinger, J., Séférian, R., Skjelvan, I., Smith, A. J. P., Sutton, A. J., Tanhua, T., Tans, P. P., Tian, H., Tilbrook, B., van der Werf, G., Vuichard, N., Walker, A. P., Wanninkhof, R., Watson, A. J., Willis, D., Wiltshire, A J., Yuan, W., Yue, X., and Zaehle, S.: Global Carbon Budget 2020, Earth Syst. Sci. Data, 12, 3269–3340, https://doi.org/10.5194/essd-12-3269-2020, 2020.

GOLLUM, 2015~~comparison~~: Manning, A. C., Keeling, R. F., Etchells, A. J., Hewitt, M., Bender, M. L., Bracchi, K., Brailsford, G. W., Brand, W. A., Cassar, N., Cox, A. C., Leuenberger, M., Meijer, H. A. J., Morimoto, S., Nakazawa, T., Neubert, R. E. M., Paplawsky, W. J., Richter, J. M., Stephens, B. B., Tohjima, Y., van der Laan, S., van der Laan−Luijkx, I. T., Watt, A., and Wilson, P. A.: The "GOLLUM" O_2 intercomparison programme: Latest results and next step, Second APO Workshop, La Jolla, California, U.S.A., 18-20 September 2015, https://gollum.uea.ac.uk/apo-2015.shtml

Glueckauf, E.: The composition of atmospheric air. Compendium of Meteorology. T. Malone. Boston, American Meteorological Society**:** 3-10, https://doi.org/10.1007/978-1-940033-70-9_1, 1951.

Goto, D., Morimoto, S., Ishidoya, S., Ogi, A., Aoki, S., and Nakazawa, T.: Development of a high precision continuous measurement system for the atmospheric O_2/N_2 ratio and its application at Aobayama, Sendai, Japan, J. Meteorol. Soc. Japan, 91, 179–192, https://doi.org/10.2151/jmsj.2013-206, 2013.

Goto, D., Morimoto, S., Ishidoya, S., Aoki, S., and Nakazawa, T.: Terrestrial biospheric and oceanic CO_2 uptakes estimated from long-term measurements of atmospheric CO_2 molar fraction, $\delta^{13}C$, and $\delta(O_2/N_2)$ at Ny-Ålesund, Svalbard, J. Geophys. Res., 122, 1192-1202, https://doi.org/10.1002/2017JG003845, 2017.

Ishidoya, S. and Murayama, S.: Development of a new high precision continuous measuring system for atmospheric O_2/N_2 and Ar/N_2 and its application to the observation in Tsukuba, Japan, Tellus B: Chem. Phys. Meteorol., 66, 22574, https://doi.org/10.3402/tellusb.v66.22574, 2014.

Ishidoya, S., Aoki, S., and Nakazawa T.: High precision measurements of the atmospheric O_2/N_2 ratio on mass spectrometer, J. Meteorol. Soc. Japan, 81, 127–140, https://doi.org/10.2151/jmsj.81.127, 2003.

Ishidoya, S., Morimoto, S., Aoki, S., Taguchi, S., Goto, D., Murayama, S., and Nakazawa, T.: Oceanic and terrestrial biospheric CO_2 uptake estimated from atmospheric potential oxygen observed at Ny-Ålesund, Svalbard, and Syowa, Antarctica, Tellus B: Chem. Phys. Meteorol., 64, 18924, /doi.org/10.3402/tellusb.v64i0.18924, 2012a.

Ishidoya, S., Aoki, S., Goto, D., Nakazawa, T., Taguchi, S., and Patra, P. K.: Time and space variations of the O_2/N_2 ratio in the troposphere over Japan and estimation of global CO_2 budget, Tellus B: Chem. Phys. Meteorol., 64, 18964, https://doi.org/10.3402/tellusb.v64i0.18964, 2012b.

Ishidoya, S., Tsuboi, K., Murayama, S., Matsueda, H., Aoki, N., Shimosaka, T., Kondo, H., and Saito, K.: Development of a continuous measurement system for atmospheric O_2/N_2 ratio using a paramagnetic analyzer and its application on Minamitorishima Island, Japan, SOL, 13, 230–234, https://doi.org/10.2151/sola.2017-042, 2017.

Junk, G. A. and Svec, H. J.: The absolute abundance of the nitrogen isotopes in the atmosphere and compressed gas from various sources, Geochim. Cosmochim. Acta, 14, 234–243, https://doi.org/10.1016/0016-7037(58)90082-6, 1958.

ISO 6142-1:2015, Gas analysis-preparation of calibration gas mixtures-part 1: gravimetric method for class i mixtures, International Organization for Standardization, ISO 6142–1:2015.

Keeling, R. F.: Development of an interferometric oxygen analyzer for precise measurement of the atmospheric O_2 mole fraction, Ph.D. thesis, Harvard University, Cambridge, 1988a

Keeling, R. F.: Measuring correlations between atmospheric oxygen and carbon-dioxide mole fractions - a preliminary-study in urban air, Journal of Atmospheric Chemistry, 7(2), 153-176, https://doi.org/10.1007/BF00048044, 1988b.

Keeling, R. F. and Shertz, S. R.: Seasonal and interannual variations in atmospheric oxygen and implications for the global carbon cycle. Nature, 358, 723–727, https://doi.org/10.1038/358723a0, 1992.

Keeling, R. F., Bender, M. L., and Tans, P. P.: What atmospheric oxygen measurements can tell us about the global carbon cycle, Global Biogeochem. Cycles, 7, 37–67, https://doi.org/10.1029/92GB02733, 1993.

Keeling, R. F., Piper, S. C., and Heimann, M.: Global and hemispheric CO_2 sinks deduced from changes in atmospheric O_2 concentration, Nature, 381, 218–221, https://doi.org/10.1038/381218a0, 1996.

Keeling, R. F., Manning, A. C., McEvoy, E. M., and Shertz, S. R.: Methods for measuring changes in atmospheric O_2 concentration and their application in southern hemisphere air, J. Geophys. Res., 103, 3381–3397, https://doi.org/10.1029/97JD02537, 1998.

Keeling, R. F., Blaine, T. Paplawsky, B, Katz, L., Atwood, C., and Brockwell, T.: Measurement of changes in atmospheric Ar/N_2 ratio using a rapid-switching, single-capillary mass spectrometer system, Tellus., 56 B, 322-338, https://doi.org/10.3402/tellusb.v56i4.16453, 2004

Keeling, R. F., Manning, A. C., Paplawsky, W. J., Cox, A.: On the long-term stability of reference gases for atmospheric O_2/N_2 and CO_2 measurements, Tellus., 59 B, 3–14, https://doi.org/10.1111/j.1600-0889.2006.00196.x, 2007.

Keeling, R. F., Walker, S. J. and Paplawsky, B.: Span sensitivity of the Scripps interferometric oxygen analyzer. SIO Reference Series, Scripps Institution of Oceanography, UC San Diego: 1-49, 2020.

Kronjäger, W.: Dispersion von Luft, Krypton und Xenon im kurzwelligen Ultraviolett, Zeitschrift für Physik 98(1-2), 17-22, https://doi.org/10.1007/BF01337441, 1936.

Langenfelds, R. L., Francey, R. J., Steele, L. P., Battle, M., Keeling, R. F., and Budd, W. F.: Partitioning of the global fossil CO_2 sink using a 19-year trend in atmospheric O_2, Geophys. Res., Lett., 26, 1897–1900, https://doi.org/10.1029/1999GL900446,1999.

Leuenberger, M. C., Schibig, M. F., and Nyfeler, P.: Gas adsorption and desorption effects on cylinders and their importance for long-term gas records, Atmos. Meas. Tch., 8, 5289–5299, doi:10.5194/amt-8-5289-20158d, https://doi.org/10.5194/amt-8-5289-2015, 2015.

Levitus, S., Antonov, J. I., Boyer, T. P., Baranova, O. K., Garcia, H. E., Locarnini, R. A., Mishonov, A. V., Reagan, J. R., Seidov, D., Yarosh, E. S., and Zweng, M. M.: World ocean heat content and thermosteric sea level change (0–2000 m), 1955–2010, Geophys. Res. Lett., 39, L10603, doi:10.1029/2012GL051106, https://doi.org/10.1029/2012GL051106, 2012.

Li, W., Ni, B., Jin, D., and Chang, T. L.: Measurement of the absolute abundance of oxygen–17 in V–SMOW, Kexue Tnbao, 33, 1610–1613, 1988.

Manning, A. C., Keeling, R. F., and Severinghaus, J. P.: Precise atmospheric oxygen measurements with a paramagnetic oxygen analyzer, Global Biogeochem. Cycles, 13, 1107–1115, https://doi.org/10.1029/1999GB900054, 1999.

Manning, A.C., and Keeling, R. F.: Global oceanic and land biotic carbon sinks from the Scripps atmospheric oxygen flask sampling network, Tellus B: Chem. Phys. Meteorol., 58, 95–116, https://doi.org/10.1111/j.1600-0889.2006.00175.x, 2006.

Matsumoto, N., Watanabe T., Maruyama, M., Horimoto Y., T. Maeda, T., Kato, K.: Development of mass measurement equipment using an electronic mass-comparator for the gravimetric preparation of reference gas mixtures, Metrologia, 41, 178-188, https://doi.org/10.1088/0026-1394/41/3/011, 2004.

Matsumoto, N., Shimosaka, T., Watanabe, T., Kato, K. : Evaluation of error sources in a gravimetric technique for preparation of a reference gas mixture (carbon dioxide in synthetic air), Anal. Bioanal. Chem., 391, 2061-2069, https://doi.org/10.1007/s00216-008-2107-8, 2008.

Rasplandy, L., Keeling, R. F., Eddebbar, Y., Brooks, M. Wang, R., Bopp, L. Long, M. C., Dunne, J. P., Koeve, W., and Oschlies, A.: Quantification of ocean heat uptake from changes in atmospheric O_2 and CO_2 composition, Nat. Res., 9, 20244, https://doi.org/10.1038/s41598-019-56490-z, 2019.

Severinghaus, J.: Studies of the terrestrial O_2 and carbon cycles in sand dune gases and in biosphere 2, Ph. D. thesis, Columbia University, New York, https://doi.org/10.2172/477735, 1995.

Stephens, B. B., Bakwin, P. S., Tans, P. P., Teclaw, R. M., and Baumann, D.: Application of a differential fuel-cell analyzer for measuring atmospheric oxygen variations, J. Atmos. Ocean. Technol., 24, 82–94, https://doi.org/10.1175/JTECH1959.1, 2007.

Stephens, B.B., Keeling, R. F., Heimann, M., Six, K. D., Mumane, R., and Caldeira, K.: Testing global ocean carbon cycle models using measurements of atmospheric O_2 and CO_2 concentration, Global Biogeochem. Cycles, 12, 213–230, https://doi.org/10.1029/97GB03500, 1998.

Stephens, B. B., Keeling, R. F., and Paplawsky, W. J.: Shipboard measurements of atmospheric oxygen using a vacuum-ultraviolet absorption technique, Tellus B: Chem. Phys. Meteorol., 55, 857–878, doi: 10.3402/tellusb.v55i4.16386, https://doi.org/10.3402/tellusb.v55i4.16386, 2003.

Sturm, P., Leuenberger, M., Sirignano, C., Neubert, R. E. M., Meiger, H. A. J., Langenfelds, R., Brand, W. A., and Tohjima, Y.: Permeation of atmospheric gases through polymer O-rings used in flasks for air sampling, J. Geophys. Res., 109, D04309, https://doi.org/10.1029/2003JD004073, 2004.

Tohjima, Y.: Method for measuring changes in the atmospheric O_2/N_2 ratio by a gas chromatograph equipped with a thermal conductivity detector, J. Geophys. Res., 105, 14575–14584, https://doi.org/10.1029/2000JD900057, 2000.

Tohjima, Y., Machida, T., Watai, T., Akama, I., Amari, T., and Moriwaki, Y.: Preparation of gravimetric standards for measurements of atmospheric oxygen and reevaluation of atmospheric oxygen concentration, J. Geophys. Res., 110, D1130, https://doi.org/10.1029/2004JD005595, 2005.

Tohjima, Y., Mukai, H., Nojiri, Y., Yamagishi, H., and Machida, T.: Atmospheric O_2/N_2 measurements at two Japanese sites: Estimation of global oceanic and land biotic carbon sinks and analysis of the variations in atmospheric potential oxygen (APO), Tellus B: Chem. Phys. Meteorol., 60, 213–225, https://doi.org/10.1111/j.1600-0889.2007.00334.x, 2008.

Tohjima, Y., Mukai, H., Machida, T., Hoshina, Y., and Nakaoka, S.: Global carbon budgets estimated from atmospheric O_2/N_2 and CO_2 observations in the western Pacific region over a 15-year period, Atmos. Chem. Phys., 19, 9269–9285, https://doi.org/10.5194/acp-19-9269-2019, 2019.

Wieser, M.E., and Berglund, M. (2009), Atomic weights of the elements 2007 (IUPAC Technical Report), Pure Appl.Chem., 81, 2131–2156.

WMO, 2005: Global Atmosphere Watch, 12th WMO/IAEA Meeting of Expert on Carbon Dioxide Concentration and Related Tracers Measurements Techniques (Toronto, Canada,15-18 September 2003). GAW Report No.161, WMO TD No. 1275, Geneva.

Table 1. The gravimetric values of N_2, O_2, Ar, and CO_2 molar fractions and $\delta(O_2/N_2)$ in five round-robin standard mixtures prepared by the NMIJ/AIST[a]

Cylinder number	*Preparation date*	*Gravimetric values*[b]				
		N_2[c]	O_2[c]	Ar[c]	CO_2[c]	$\delta(O_2/N_2)$[d]
CPB16345	April 7, 2017	781499.1 ± 1.0	208750.7 ± 0.8	9349.6 ± 0.7	400.43 ± 0.03	−3582.2 ± 4.0
CPB16315	April 12, 2017	781264.6 ± 0.9	209040.2 ± 0.7	9297.0 ± 0.7	398.18 ± 0.03	−1901.1 ± 3.8
CPB16379	April 17, 2017	781059.4 ± 0.8	209233.2 ± 0.7	9308.6 ± 0.6	398.68 ± 0.03	−716.9 ± 3.3
CPB28912	June 15, 2017	780792.2 ± 0.8	209437.1 ± 0.7	9351.1 ± 0.6	419.44 ± 0.03	599.2 ± 3.4
CPB16349	June 13, 2017	780424.6 ± 0.8	209813.5 ± 0.7	9342.7 ± 0.6	419.06 ± 0.03	2869.7 ± 3.4

[a] The high-precision standard mixtures were prepared in a previous study (Aoki et al., 2019). However, the gravimetric values of N_2, O_2, Ar, and CO_2 molar fractions were recalculated based on the cylinders' expansion rate, which was determined by measuring change of water volume with depletion of inner pressure of the cylinders sunk in water from 110 bar to 1 bar. The value was determined as 1.62 ± 0.06 ml MPa^{-1} by our experiment (unpublished data) and used to correct buoyancy of cylinders.

[b] The numbers following the symbol ± denote the standard uncertainty of the gravimetric value which was calculated according to the law of propagation of uncertainties.

[c] Figures are given in the unit of μmol mol^{-1} in dry air.

[d] Figures are given in the unit of per meg. These values were calculated against the O_2/N_2 ratio which assigned zero on the NMIJ/AIST scale to correspond to a ratio in the atmosphere value in 2015 (0.2093391/ 0.7808943 = 0.2680761) (Aoki et al., 2019).

Table 2. Measurement techniques, measurement species, and reported values of EMRI/AIST, NIES, TU, and SIO.

Constituent	*EMRI/AIST*	*NIES*	*TU*	*SIO*
Analysis period	May–July 2017	Sep–Nov 2017	Dec 2017–Jan 2018	May–Nov 2018
Measurement technique	Mass spectrometry	Gas chromatography	Mass spectrometry	Interferometric method
Measurement species	$^{14}N^{14}N$, $^{15}N^{14}N$, $^{16}O^{16}O$, $^{17}O^{16}O$, $^{18}O^{16}O$	O_2, N_2, Ar	$^{16}O^{16}O$, $^{14}N^{15}N$	O_2 (interferometer)
Reported values	$\delta(^{16}O^{16}O/^{14}N^{14}N)$[a]	$\delta(O_2/N_2)$	$\delta(^{16}O^{16}O/^{15}N^{14}N)$[a]	$\delta(O_2/N_2)$

[a] The $\delta(O_2/N_2)$ values of EMRI/AIST and TU were computed using $\delta(^{17}O/^{16}O)$, $\delta(^{18}O/^{16}O)$, and $\delta(^{15}N/^{14}N)$ measured by EMRI/AIST (see text). CO_2 molar fractions measured by EMRI/AIST were used to correct $\delta(^{16}O^{16}O/^{15}N^{14}N)$ values.

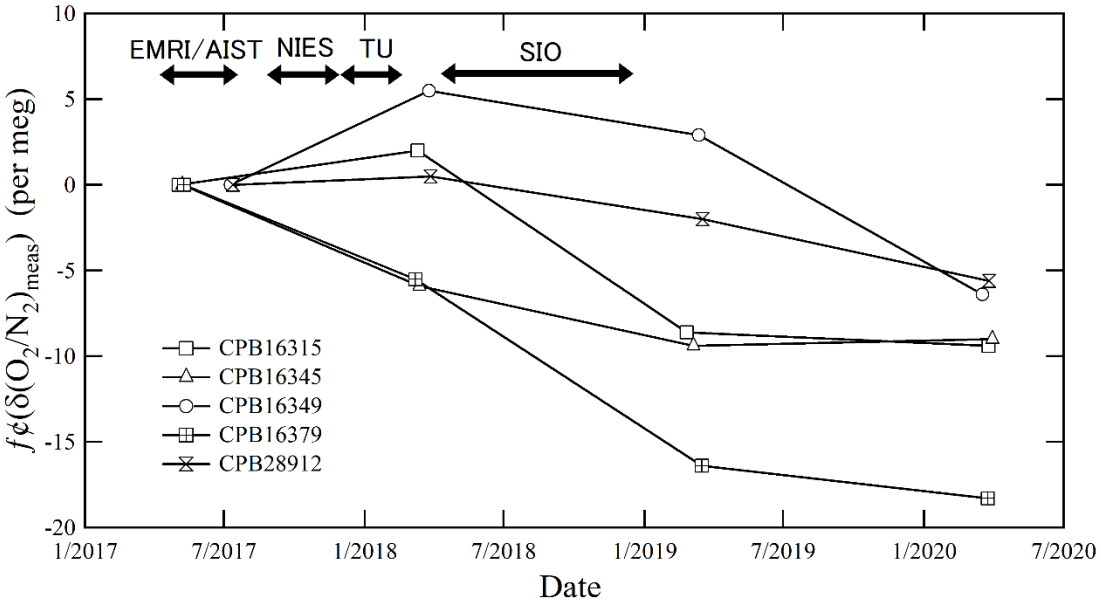

Figure 1 The temporal drift of $\delta(O_2/N_2)_{round\text{-}robin}$ values from the initial values was measured using a mass spectrometer at EMRI/AIST after preparing the round-robin standard mixtures before the shipment of the cylinders to SIO, after the return of the cylinders from SIO, and a year after the return.

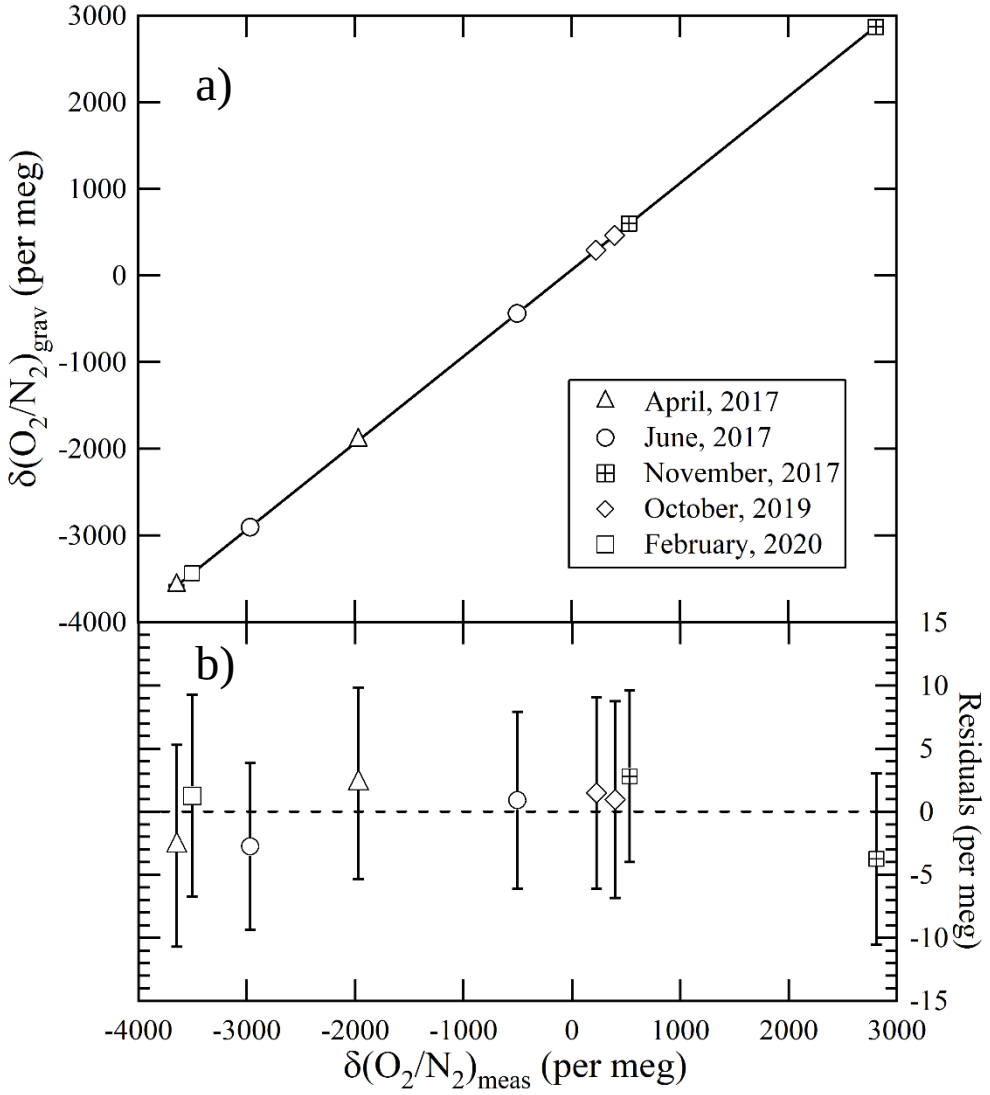

Figure 2 a) Relationships between the gravimetric values of $\delta(O_2/N_2)$ in nine high-precision standard mixtures prepared from April 2017 to February 2020 and the $\delta(O_2/N_2)$ values measured using the mass spectrometer at EMRI/AIST. b) Residuals from the line of the Deming least-square fit to the plots. Error bar represents the expanded uncertainty of the $\delta(O_2/N_2)_{NMIJ/AIST}$ values.

Table 3 $\delta(O_2/N_2)_{round\text{-}robin}$ values in the round-robin standard mixtures reported by EMRI/AIST, NIES, TU, and SIO.

Cylinder number	*EMRI/AIST*	*NIES*	*TU*	*SIO*
CPB16345	−3647.7 ± 3.2	−3858.7 ± 5.0	−4014.6 ± 5.4	−4141.7 ± 3.3
CPB16315	−1970.2 ± 3.2	−2227.0 ± 5.0	−2331.2 ± 5.4	−2485.7 ± 3.3
CPB16379	−786.6 ± 3.2	−1086.3 ± 5.0	−1149.4 ± 5.4	−1313.4 ± 3.3
CPB28912	531.5 ± 3.2	182.4 ± 5.0	177.9 ± 5.4	−0.4 ± 3.3
CPB16349	2810.2 ± 3.2	2389.2 ± 5.0	2449.5 ± 5.4	2253.5 ± 3.3

Numbers are given in the unit of per meg. The numbers following the symbol ± denote the standard uncertainty which was calculated based on measurement standard uncertainty of $\delta(O_2/N_2)$ for individual laboratories. $\delta(O_2/N_2)_{round\text{-}robin}$ values reported by individual laboratories were determined based on their own scales.

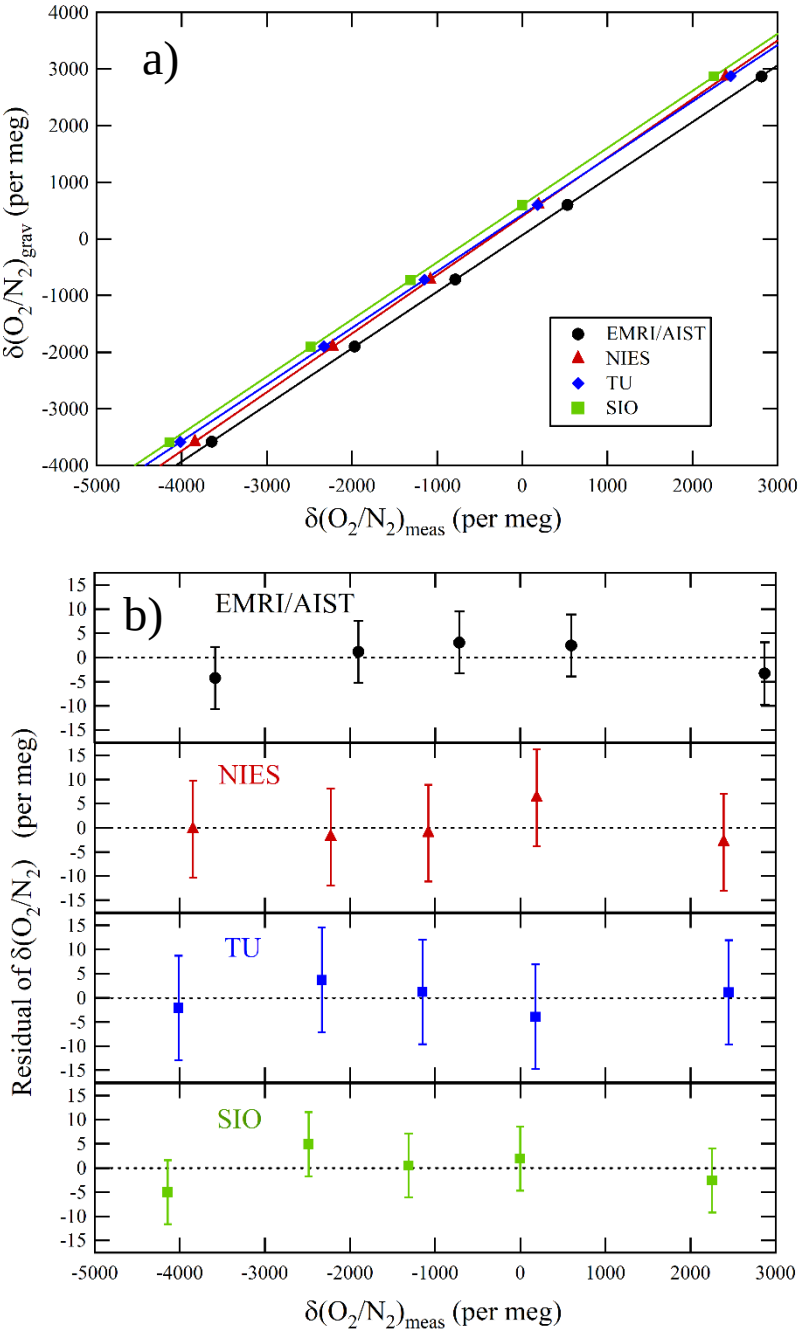

Figure 3 a) Relationships between the gravimetric $\delta(O_2/N_2)$ values by NMIJ/AIST and the $\delta(O_2/N_2)$ values measured by EMRI/AIST, NIES, TU, and SIO and lines obtained from the Deming least-square fit to the plotted data. b) Residuals of the measured $\delta(O_2/N_2)$ values from the lines. Error bar represents expanded uncertainty which was calculated based on the measurement uncertainty for individual laboratories.

Table 4. Slopes and intercepts of the lines obtained by the Deming least-square fit to the reported $\delta(O_2/N_2)_{round\text{-}robin}$ values for individual laboratories, and deviation in the individual scales from SIO in this study and the GOLLUM.

Institutes	Slopes (a_n)[a]	Intercepts (b_n)[b,c]	Deviation in individual scale from SIO scale[c,d]	Deviation from SIO values in the GOLLUM[c,e]
EMRI/AIST	0.9989 ± 0.0010	65.8 ± 2.2	−530.6 ± 3.3	—
TU	0.9990 ± 0.0013	425.7 ± 3.1	−170.8 ± 3.9	−160 ± 10.8
NIES	1.0339 ± 0.0013	404.5 ± 3.0	−191.9 ± 3.9	−195 ± 10
SIO	1.0093 ± 0.0010	596.4 ± 2.4	–	0

Numbers following the symbol ± denote the standard uncertainty. The uncertainties of slopes and intercepts were calculated based on the Deming least-square fit.

[a] Slope represents the difference in span sensitivity between individual laboratory scales and the NMIJ/AIST scale.

[b] Intercept represents a deviation in individual laboratory scale from the NMIJ/AIST scale corresponding to $\delta(O_2/N_2)_{NMIJ/AIST} = 0$.

[c] Figures are given in the unit of per meg.

[d] Standard uncertainties were calculated by combining the standard uncertainties of the individual laboratory intercepts.

[e] Figures were provided by Andrew Manning (GOLLUM, 2015, WMO, 2003, and A. Manning personal communication). EMRI/AIST did not participate in the GOLLUM.

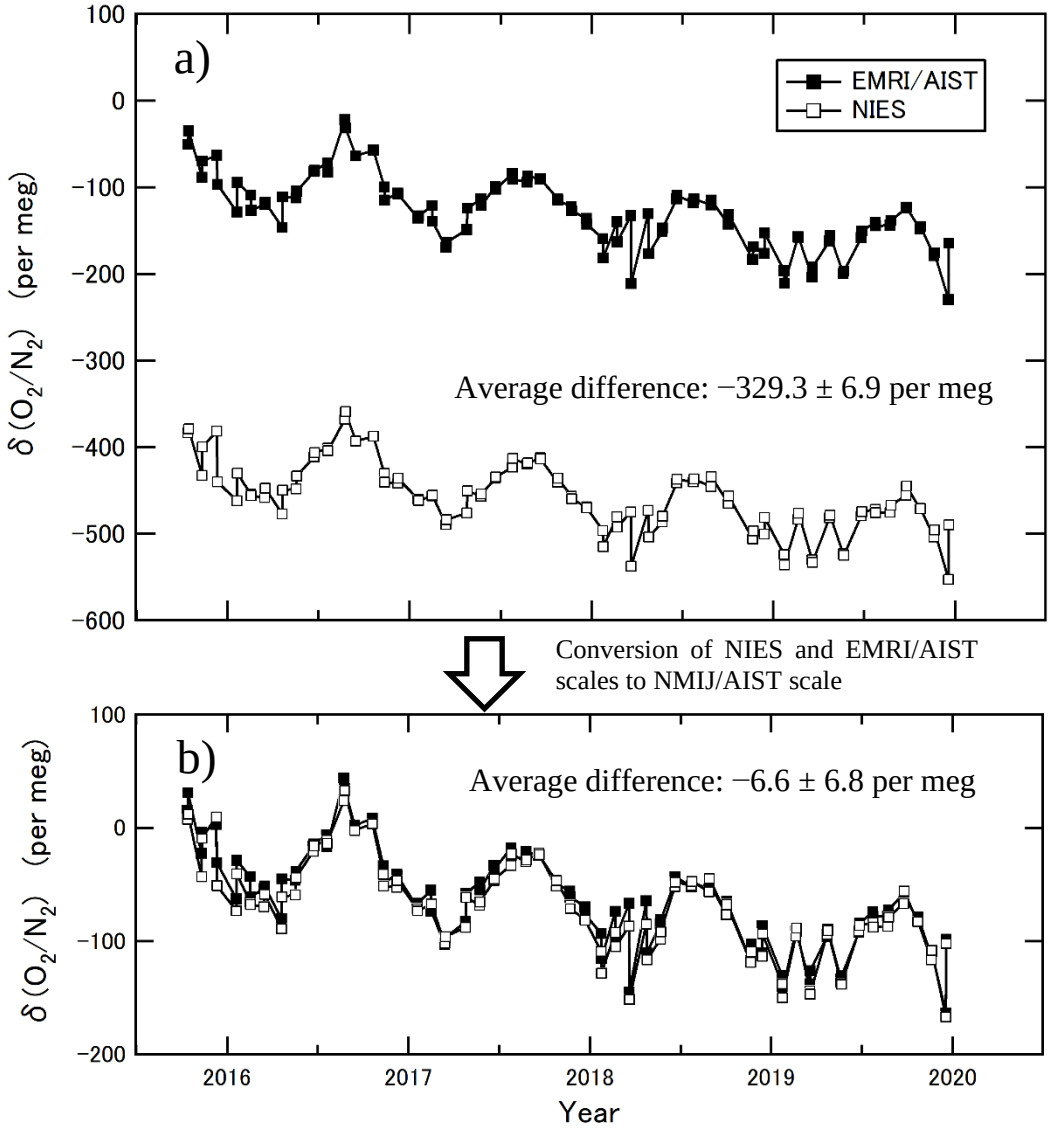

Figure 4 a) The $\delta(O_2/N_2)$ values obtained from the duplicate air samples collected at Hateruma Island for four years (2015–2019) measured by EMRI/AIST and NIES. b) The $\delta(O_2/N_2)$ values at Hateruma converted from EMRI/AIST and NIES scales to the NMIJ/AIST scale.

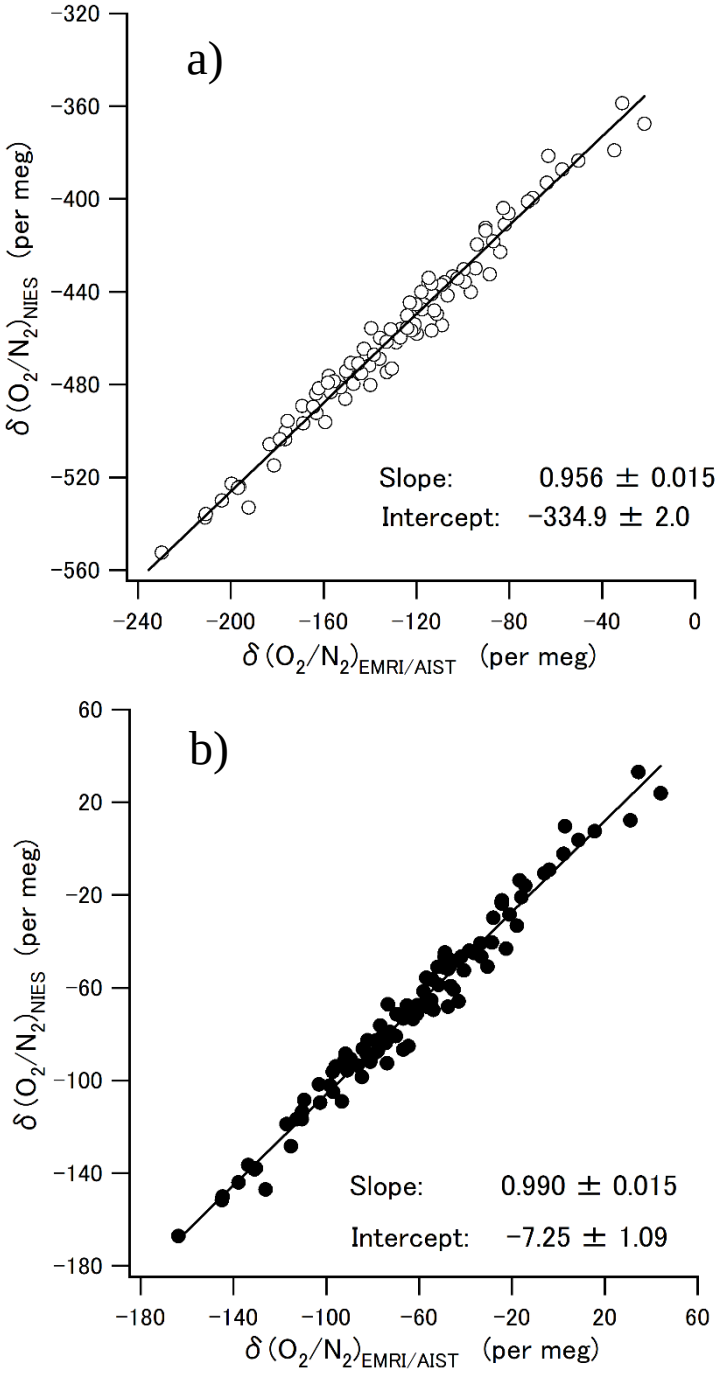

Figure 5 a) Scatter plots of the $\delta(O_2/N_2)$ values at Hateruma for four years (2015–2019) on the EMRI/AIST and NIES scales. The line represents the Deming least-square fit to the plots. b) Scatter plots between the $\delta(O_2/N_2)$ values for EMRI/AIST and NIES after conversion to the NMIJ/AIST scale. The line represents the Deming least-square fit to the plots.

Table 5. Land biospheric and oceanic CO_2 uptakes from 2000 to 2016 reported by Tohjima et al. (2019) using the NMIJ/AIST and NIES O_2/N_2 scales (see text for more details).

	Fossil fuel[a]	Atm. CO_2[a]	Land uptake	Ocean uptake
NMIJ/AIST scale	8.50	4.47	1.20[b]	2.85[b]
NIES scale			1.50 (0.91)[c]	2.55 (0.73)[c]

Figures are given in units of PgC yr^{-1}

[a] These figures were from the Global Carbon Project (Friedlingstein et al., 2020).

[b] NMIJ/AIST values were recalculated based the average secular changing rate of $\delta(O_2/N_2)$ converted from the NIES scale to the NMIJ/AIST scales.

[c] NIES values were computed based on the average secular changing rate of $\delta(O_2/N_2)$ on the NIES scale reported by Tohjima et al. (2019). The figures in parentheses represent the uncertainties.